Waste Management 85 (2019) 529–537

Contents lists available at ScienceDirect

Waste Management

journal homepage: www.elsevier.com/locate/wasman

A process for combination of recycling lithium and regenerating graphite from spent lithium-ion battery

Yue Yang [a,b], Shaole Song [a], Shuya Lei [a], Wei Sun [a,b,*], Hongshuai Hou [c], Feng Jiang [a], Xiaobo Ji [c,*], Wenqing Zhao [a], Yuehua Hu [a,b,*]

[a] School of Minerals Processing and Bioengineering, Central South University, Changsha 410083, China
[b] Key Laboratory of Hunan Province for Clean and Efficient Utilization of Strategic Calcium-containing Mineral Resources, Central South University, Changsha 410083, China
[c] College of Chemistry and Chemical Engineering, Central South University, Changsha 410083, China

ARTICLE INFO

Article history:
Received 5 November 2018
Revised 4 January 2019
Accepted 6 January 2019

Keywords:
Spent lithium ion battery
Spent anode material
Lithium recycling
Graphite regeneration

ABSTRACT

Recycling lithium and graphite from spent lithium-ion battery plays a significant role in mitigation of lithium resources shortage, comprehensive utilization of spent anode graphite and environmental protection. In this study, spent graphite was firstly collected by a two-stage calcination. Secondly, under the optimal conditions of 1.5 M HCl, 60 min and solid-liquid ratio (S/L) of 100 $g{\cdot}L^{-1}$, the collected graphite suffers simple acid leaching to make almost 100% lithium, copper and aluminum in it into leach liquor. Thirdly, 99.9% aluminum and 99.9% copper were removed from leach liquor by adjusting pH first to 7 and then to 9, and thenthe lithium was recovered by adding sodium carbonate in leach liquor to form lithium carbonate with high purity (>99%). The regenerated graphite is found to have high initial specific capacity at the rate of 37.2 $mA{\cdot}g^{-1}$ (591 $mAh{\cdot}g^{-1}$), 74.4 $mA{\cdot}g^{-1}$ (510 $mAh{\cdot}g^{-1}$) and 186 $mA{\cdot}g^{-1}$ (335 $mAh{\cdot}g^{-1}$), and with the high retention ratio of 97.9% after 100 cycles, it also displays excellent cycle performance at high rate of 372 $mA{\cdot}g^{-1}$. By this process, copper and lithium can be recovered and graphite can be regenerated, serving as a sustainable approach for the comprehensive utilization of anode material from spent lithium-ion battery.

© 2019 Elsevier Ltd. All rights reserved.

1. Introduction

Lithium ion battery (LIB) has been widely applied in consumer electronics (e.g. cameras, laptops, mobile phones, etc.), energy storage, electric vehicles (EVs), plug-in electric vehicles (PEVs) and other fields (e.g. aerospace industry, robot, etc.) due to its high energy density, good cycle performance and high discharging capacity (Li et al., 2016; Tripathi et al., 2018). It is reported that the value of global LIB market is projected to reach $50 billion by 2020 (Zou et al., 2013). The increase in the number of LIBs has also brought numerous spent LIBs. It is estimated that the quantity of spent LIBs only in China will be 25 billion units weighing 500,000 metric tons by 2020 (Li et al., 2017). As spent LIBs contain many valuable metals and lead to environmental pollution (Gomaa et al., 2018; Gao et al., 2017), recycling spent LIBs has been attracting extensive attention. Many processes have been focused on recovering metal values from spent cathode materials (Chen et al., 2018; Sattar et al., 2019). Valuable metals, such as lithium, nickel, cobalt, manganese and aluminum, can be successfully recovered from various spent cathode materials (e.g. $LiCoO_2$, $LiNi_xCo_yMn_{1-x-y}O_2$ ($0 < x, y < 1$) or $LiFePO_4$, etc.) through pyrometallurgy or hydrometallurgy methods (Yang et al., 2018a; Gao et al., 2018). At present, production lines, including pyrometallurgy and hydrometallurgy, for cathode material recovery have been set up in Europe, America and China (Yang et al., 2018b; Lv et al., 2018a), however, few previous works paid attention to recover resources from spent anode materials (Lv et al., 2018b).

In fact, recovering graphite from spent anode materials enjoys great significance in expanding the supply and alleviating the shortage of graphite resources. On one hand, being widely used in LIBs, metallurgy, atomic energy industry and other fields, graphite has been considered as one of the most important strategic materials (Hou et al., 2017). It is reported that the demand for high quality flake graphite grows by 10–12% per year (Shaw, 2012; Badawy, 2016). The price of graphite of battery grade was high up to $5000–20,000 per ton in 2016 (Badawy, 2016). Recycling spent graphite will be an inevitable choice, especially for countries which restrict the exploitation but only depend on importing graphite. On the other hand, the content of graphite in spent LIBs ranges from 12 wt% to 21 wt% and thus the amount of waste

* Corresponding authors.
E-mail addresses: sunmenghu@csu.edu.cn (W. Sun), xji@csu.edu.cn (X. Ji), huyuehuacsu@126.com (Y. Hu).

https://doi.org/10.1016/j.wasman.2019.01.008
0956-053X/© 2019 Elsevier Ltd. All rights reserved.

graphite is considerably large with the increase of spent LIBs (Moradi and Botte, 2016). Last but not least, spent anode material always contains some toxic chemicals, such as electrolyte (Rothermel et al., 2016). Therefore, recycling spent graphite will not only recover resources but also eliminate pollution.

Some studies report on comprehensive utilization of graphite from spent LIBs. Spent graphite is firstly separated from spent LIBs by physical methods, including dismantling, crushing, screening, and other mechanical processes (Yang et al., 2016a, 2016b). And then, the separated graphite can be used as the raw material of preparing graphene or other functional materials. Zhao et al. prepared MnO_2-modified graphite sorbent from spent LIBs and then used the sorbent to treat the waste water contaminated by lead, cadmium, and silver (Zhao et al., 2017). Cao et al. reused anode scrap from lithium-ion batteries as the cathode of pollutant degradation. When anode powder is reused in electro-Fenton system, Al electrode achieves 100% bisphenol A (BPA) removal in 70 min and 87.4% COD removal in 240 min (Cao et al., 2018). Some progress has been made on the recovery of spent graphite. However, the effective way for large-scale recycling of scrap graphite from spent LIBs is still unavailable. One of the most important problems is that less attention is paid to lithium recovering from spent anode graphite. In fact, lithium concentration in spent anode graphite is much higher that required by environmental standards (Cao et al., 2018). According to statistics by USGS, lithium production all over the world increased by 13% to 43,000 tons in 2017 due to growing lithium demand for battery applications (U.S. Geological Survey, 2018). In China, the price of spot lithium carbonate increased from $15,000 to $24,000 per ton (U.S. Geological Survey, 2018). Therefore, recovering lithium from spent anode graphite can not only alleviate the shortage of lithium resources, but also make the comprehensive utilization of spent anode graphite more cost-efficient.

With typical layer structure, the theoretical capacity of graphite is high up to 372 $mAh{\cdot}g^{-1}$ (Wen et al., 2015; Schweidler et al., 2018). For the high value-added recycling of spent graphite by short process, an important challenge calling for urgent solution is to recover lithium and rejuvenate the electrochemical properties of graphite. In this study, a new process for graphite regeneration has been developed. By this process, copper, lithium and anode graphite can be recovered successively and the comprehensive utilization of anode materials from spent LIBs can be achieved.

2. Experimental

2.1. Materials and reagents

Reagents for all experiments are of analytical grade. Hydrochloric acid, sodium hydroxide and sodium carbonate were bought from Xilong Reagent Corporation of China. Deionized water was used to prepare solutions. Spent anode material graphite was obtained from spent LIBs of automotive electronics and computers. Before being dismantled, spent LIBs were discharged in salt water for 8 h. And then anode current collectors were selected manually.

2.2. Lithium and graphite recycling

The obtained anode current collectors were firstly treated under the protection of high purity argon (80 $ml{\cdot}min^{-1}$, degree of purity > 99.999%) in a tube furnace (Ke Jing, GSL-1100X-S). Rothermel et al. has analyzed the TG-DSC measurement of spent graphite. The results show that electrolyte volatilizes and carboxyl groups of binder decompose when temperature reaches around 400 °C (Rothermel et al., 2016). Therefore, graphite was separated from copper foils at 400 °C for 1 h under argon protection. And then the copper foils were recovered directly (Fig. S1), while the separated graphite was further treated at 500 °C for 1 h in a muffle furnace in air atmosphere (Ke Jing, 1200X-J) to oxidize the metal copper in graphite into copper oxide. To detect the composition of obtained graphite, 5 g graphite was leached in the mixture of 1 M hydrochloric acid and 4% hydrogen peroxide solution at 80 °C for 2 h. Then, the left graphite was dried, filtrated and weighted. The leaching solution was tested by ICP-OES. The contents of lithium, aluminum and copper in spent graphite are 0.47 wt%, 0.33 wt% and 0.59 wt%, respectively (Table S1). The graphite recovery process was performed in a 500 ml separating funnel fixed on a vibrator (Fig. S2). The details and flowsheet can be found in Fig. S3.

Lithium left in leach liquor was recovered by sodium carbonate precipitation method. Before lithium recycling, leach liquor was purified to remove copper and aluminum. 100 ml leach liquor was put into a 250 ml round-bottom flask. Sodium hydroxide with a concentration of 2 M was dropped into the leach liquor under magnetic stirring (100 rpm) at room temperature to adjust pH value. After the reaction under a certain pH, the obtained solid-liquid mixture was separated by filtration. Then, the concentration of lithium in filtrate was adjusted to 1 M by evaporation. 0.5 M sodium carbonate solution was added into the filtrate with the feed rate of 2 $ml{\cdot}min^{-1}$ under magnetic stirring (300 rpm). Reaction temperature was kept at 80 °C. The precipitate was firstly filtered and washed by distilled water to completely remove chloridion and sodium ions, and then dried at 80 °C in a vacuum oven for 8 h. The whole process can be seen in Fig. 1.

2.3. Measurement and characterization

The phases of obtained copper foil, spent graphite before and after thermal treatment, and the recycled products were analyzed with powder X-ray diffraction (XRD, Rigaku-2000) using Cu Kα radiation by a step size of 0.02° at a scan rate of $2°{\cdot}min^{-1}$. The C 1s spectra of regenerated graphite was measured by X-ray photoelectron spectroscopy (XPS, ESCALAB 250Xi). The composition of metal ions in liquid was measured by an inductively coupled plasma atomic emission spectrometry (VARIAN, VISTA-MAPX CCD, ICP-OES). Leaching efficiency was determined by material balance. The surface area and pore size of spent graphite were calculated with Brunauer-Emmett-Teller (BET) method and Barrett-Joyner-Halenda (BJH) method using a specific surface area and porosity analyzer (Quantachrome, NOVA 3200e). The morphologies and composition of spent graphite before and after leaching were measured by a scanning electron microscope (SEM, FEI Quanta 250) and energy dispersive X-ray spectroscopy system (EDXS, Thermo).

Electrochemical performances of regenerated graphite were tested by using coin cells. 90 wt% regenerated graphite, 5 wt% acetylene black and 5 wt% polyvinylidene fluoride were firstly mixed to form a uniform slurry. The slurry was coated on a copper foil and dried at 80 °C for 8 h in a vacuum oven, before being punched into cake-shape plate. The plate functioned as working electrode, lithium metal foil as counter electrode, celgard 2400 polyethylene/polypropylene as separator, and the mixture of 1 M $LiPF_6$ of dimethyl carbonate (DMC) and ethylene carbonate (EC) (DMC:EC = 1:1 in molar ratio) as electrolyte. Type Coin cell of CR2032 was arranged in a glovebox under the protection of argon. A battery test system (LAND-CT2001A, China) was used to test the electrochemical performances of prepared cell in voltage range of 0.005–2 V at 25 °C. Electrochemical impedance spectroscopy (EIS) was pweformed at a Princeton Workstation (Parstat2273) in the frequency range from 1 MHz to 0.01 Hz at AC voltage of 5 mV.

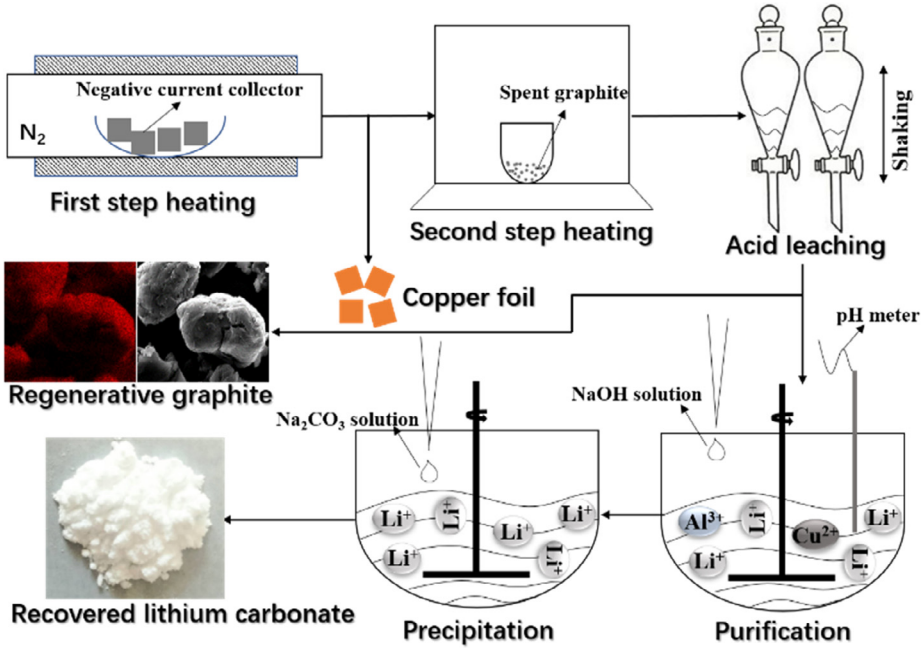

Fig. 1. Flow chart of the whole recycling process.

3. Result and discussion

3.1. Thermal treatment

As seen from Fig. 2(a), anode current collector mainly consists of current collector (copper foil), active material (graphite), conductive additive (acetylene black) and binder. Graphite was bonded on the surface of copper foil by binder polyvinylidene fluoride (PVDF) or polytetrafluoroethylene (PTEF). As the pyrolysis temperature of binder is much lower than the melting temperature of copper (Alhusaiki, 2017; Lewis and Naylor, 1947), the binder can be removed without damaging copper, and the separation of copper and graphite can be achieved when temperature was controlled between the pyrolysis temperature of binder and the melting temperature of copper, i.e. 400 °C. The recycled coper foils can be found in Fig. S1, and the XRD pattern of recovered copper after thermal treatment at 400 °C for 1 h under the protection of high purity argon can be seen in Fig. 2(b). Fig. 2(b) shows that two peaks at around 44° and 50° are attributed by copper structure. In addition, no characteristic peaks of graphite, copper oxide or cuprous oxide are observed, indicating that the obtained copper is pure and can be recycled without any further treatment.

In the process of dismantling spent LIBs and then separating copper foils and graphite by thermal treatment, the aluminum in positive current collector and the copper in anode current collector will inevitably enter into spent graphite (Fig. 2(c)). To regenerate graphite, the impurities copper and aluminum must be removed. Aluminum can be easily and selectively leached from spent graphite by sulfuric acid or hydrochloric acid solution, while it is difficult for metal copper to react with acid in absence of oxygen (Altass et al., 2016). Metal copper can be dissolved in acid solution with the help of oxidizing agent, but the consumption of oxidizing agent increases leaching costs. In this case, metal copper was oxidized by oxidizing roasting. The metal copper in spent graphite, suffering thermal treatment at 400 °C for 1 h under the protection of high purity argon, can be easily oxidized to copper oxide at 500 °C for 1 h under air atmosphere (Fig. 2(d)). It is reported that the electrolyte volatilizes and decomposes during the pyrolysis process (Rothermel et al., 2016). The harmful gases, such as hydrogen fluoride, organic compounds including ethylene carbonate, propylene carbonate or diethyl carbonate and their decomposed product, will be generated in the process of thermal treatment. However, these pollutions can be effectively eliminated by mature technology of alkali absorption followed by activated carbon adsorption (Senćanski et al., 2017; Xiao et al., 2017).

3.2. Leaching

After oxidizing roasting, the metals in spent graphite can be easily leached in hydrochloric solution. The leaching behaviors of lithium, copper and aluminum under various conditions are displayed in Fig. 3. As shown in Fig. 3(a), the leaching efficiencies of lithium, copper and aluminum increase with the concentration of hydrochloric acid increasing, and the leaching efficiencies of the three metals reach the maximum at the hydrochloric acid concentration of 1.5 M. Fig. 3(b) shows effect of leaching time on metal recovery efficiency With reaction time increasing, the leaching efficiencies of lithium, copper and aluminum firstly increase, and then decrease under leaching conditions of 1.5 M HCl and S/L = 20 $g{\cdot}L^{-1}$. It is reported that graphite can absorb metal ions in acid solution (Xu et al., 2018), so the leached ions in solution may be re-absorbed by graphite with leaching time prolonging, resulting in leaching efficiency decrease. Consequently, the optimal leaching time is determined as 60 min, and the leaching efficiencies of lithium, copper and aluminum reach almost 100%. Fig. 3(c) displays the influence of S/L on metal recovery efficiency under leaching conditions of 1.5 M HCl and 60 min. Due to the low density of spent graphite, a small amount of acid solution can not completely infiltrate the graphite. As a result, the recovery efficiencies of lithium, copper and aluminum are low at a high S/L. But when S/L reduces to S/L = 100 $g{\cdot}L^{-1}$, the recovery efficiencies of lithium, copper and aluminum reach almost 100%, 98.5%, and 99.2%, respectively. Therefore, the optimal conditions for leaching lithium, copper and aluminum from spent graphite is 1.5 M HCl, 60 min and S/L = 100 $g{\cdot}L^{-1}$. Fig. 3(d) shows the XRD patterns of spent graphite before and after leaching process under the optimal leaching conditions. As seen in Fig. 3(d), the characteristic peaks of impurities disappear and the peaks of obtained leaching residue at

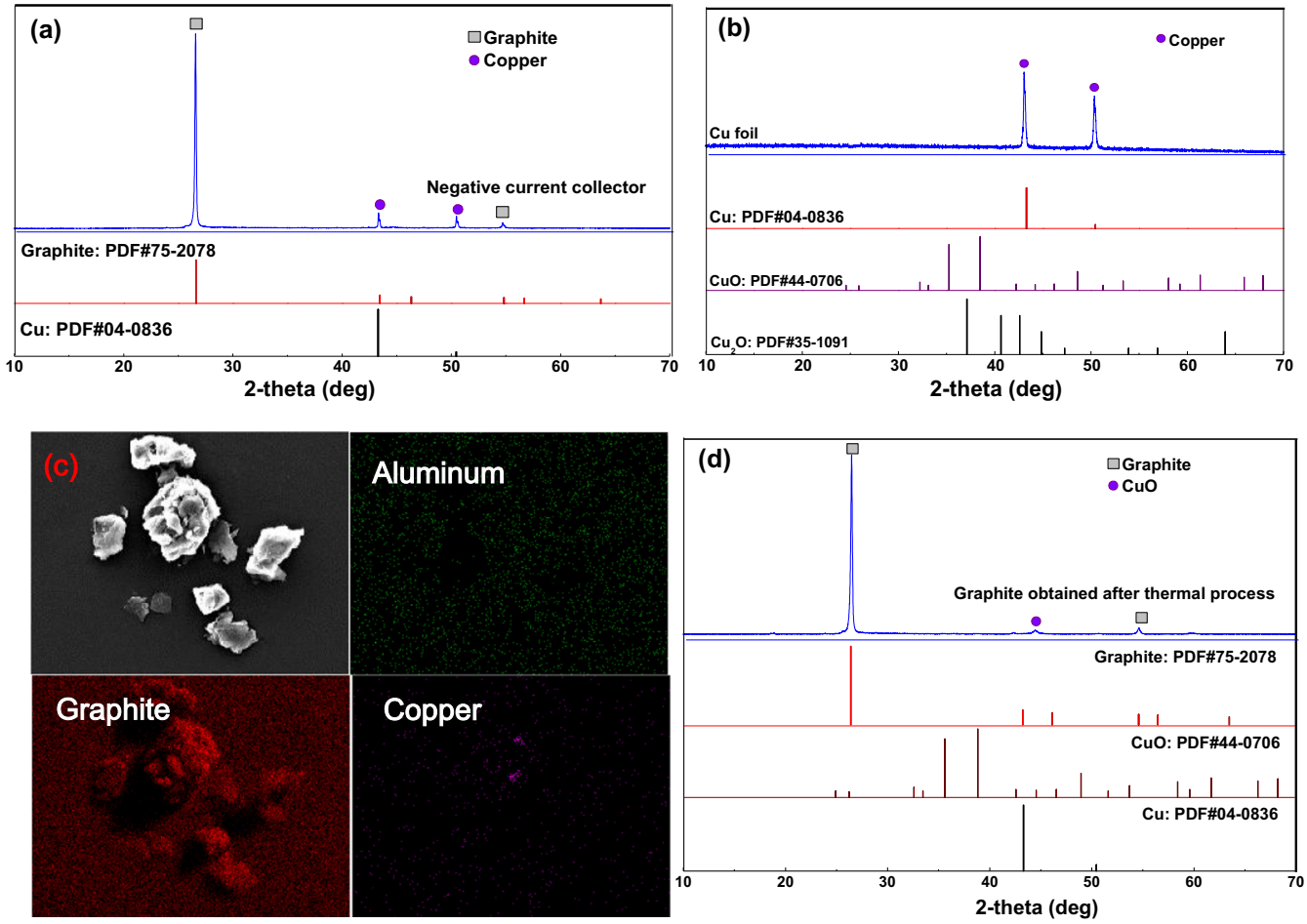

Fig. 2. (a) XRD pattern of anode current collectors, (b) XRD pattern of the copper foil obtained after thermal treatment at 400 °C for 1 h under the protection of high purity argon, (c) EDX spectroscopy of graphite collected after thermal treatment at 400 °C for 1 h under the protection of high purity argon, (d) XRD pattern of the graphite obtained after oxidizing roasting at 500 °C for 1 h under the air atmosphere.

around 26.7° and 54.9° match exactly with that of standard graphite. The content of obtained graphite tested by ICP-OES (Table S1) further proves that the lithium, copper and aluminum have been successfully removed and pure graphite has been obtained. XPS measurement suggested that a strong peak corresponding to C—C/C=C bonds can be found at around 284.8 eV (Sun et al., 2018) and no other peak exists (Fig. S4), which further means that the pure graphite was regenerated.

3.3. Lithium recovery

After acid leaching, the concentrations of lithium, copper and aluminum in leach liquor are 470 mg·L^{-1}, 585 mg·L^{-1} and 325 mg·L^{-1}, respectively. To regenerate lithium from leach liquor, impurities copper and aluminum must be removed. Fig. 4 shows the relation between pH value and copper, and aluminum and lithium species in leaching solution. As seen in Fig. 4(a), almost all copper ions can be converted to precipitate when pH is kept at 8–9. For aluminum, its hydrolysis is also greatly influenced by varying pH value (Fig. 4(b)). Aluminum initially forms positively charged colloidal precipitate at neutral pH, and then the precipitate aggregates grow into large particles as pH increases (Duan and Gregory, 2003). It is also reported that Al^{3+} tends to form aluminum hydroxide precipitate in the neutralization of $AlCl_3$ solutions with intense mixing, and a minimum solubility of 1 μM can be achieved at pH of 6–8, although polynuclear hydrolysis products, such as $Al(OH)^{2+}$, and $Al(OH)_2^+$, exist in theoretical calculation when aluminum hydroxide precipitate appears (Duan and Gregory, 2003; Clark et al., 1993). Therefore, the impurities copper and aluminum in leach liquor can be removed by simply adjusting pH without precipitating lithium ion (Fig. 4(c)). Based on above analysis, a precipitation experiment on a slow dropwise addition of NaOH solution with the rate of addition is 5 ml·min^{-1} using 50 ml burette was carried out. The pH value of leach liquor was firstly adjusted to 7 and kept at this value for 1 h to remove aluminum. Then, further adjust pH value to 9, and maintain it for 1 h to remove copper. Fig. 4(d) shows precipitation experiment results. Both removal efficiencies of aluminum and copper can reach above 99.9%, while the loss ratio of lithium is only around 15%. After removing impurities aluminum and copper, lithium concentration is 400 mg·L^{-1}, and both of the concentrations of aluminum and copper were below 0.5 mg·L^{-1}, which can meet the requirement for preparing lithium carbonate.

After purification, the lithium left in leach liquor was recovered by carbonate precipitation method (Pankaj et al., 2017; Yang et al., 2017). Fig. 5 shows the XRD pattern of recycled lithium carbonate. The characteristic peaks of recovered product match exactly with that of standard spectra of lithium carbonate (PDF#22-1141), and no impurity peaks were found, indicating that pure lithium carbonate was successfully recovered. To further test its purity, the recycled lithium carbonate was firstly dissolved in 2 M sulfuric acid solution, and then measured with ICP-OES. The result shows that the purity of recovered lithium carbonate is over 99%.

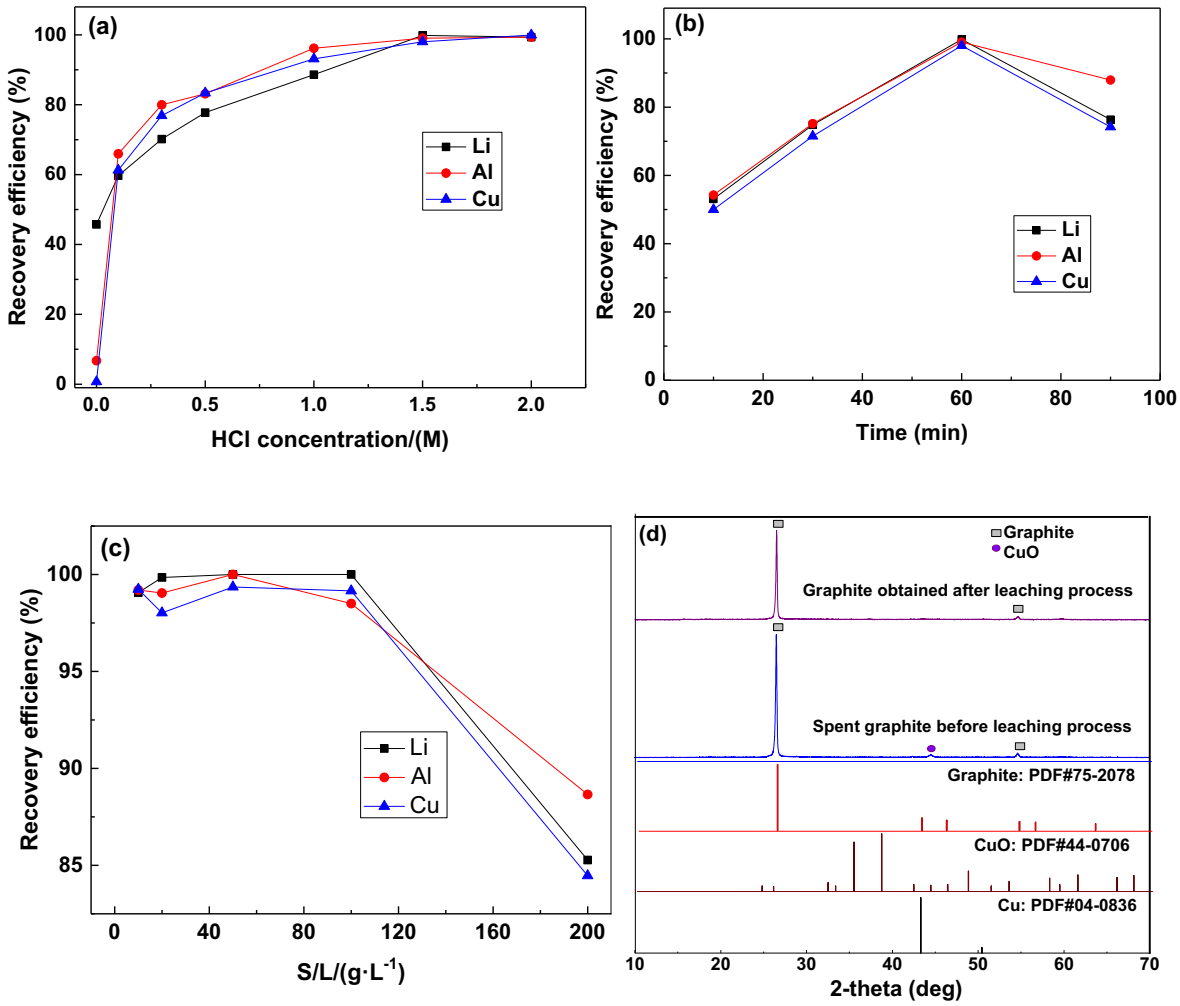

Fig. 3. The leaching behavior of lithium, copper and aluminum from the spent graphite obtained after oxidizing roasting at 500 °C for 1 h under air atmosphere at room temperature. (a) effect of HCl concentration on metal recovery efficiency under leaching conditions of S/L = 20 g·L^{-1} and 60 min, (b) effect of leaching time on metal recovery efficiency under leaching conditions of 1.5 M HCl and S/L = 20 g·L^{-1}, (c) effect of S/L on metal recovery efficiency under leaching conditions of 1.5 M HCl and 60 min, and (d) the XRD patterns of spent graphite before leaching process and graphite obtained after leaching process under the condition of 1.5 M HCl, 60 min and S/L = 20 g·L^{-1}.

3.4. Graphite recycling

Fig. 6(a)–(g) show the SEM image of graphite before and after leaching process. After thermal treatment at 500 °C for 1 h under air atmosphere, the spent graphite shows irregular particles varying in size from 10 to 50 μm (Fig. 6(a)). Compared to the spent graphite collected from anode current collector, the particle size of recycled graphite is smaller r due to acid exfoliation (Fig. 6(b)–(g)). Meanwhile, only graphite is observed in the EDXS mapping of recovered graphite (Fig. 6(e)), further indicating that the impurities, such as aluminum and copper, have been completely removed and pure graphite is obtained.

Although the particles of recycled graphite get thinner, the surface area decreases. As seen in Fig. 6(h), BET surface area of graphite is reduced from 7.0 m^2/g to 2.6 m^2/g after acid leaching under the condition of 1.5 M HCl, 60 min and S/L = 100 g·L^{-1}. The decrease of surface area may be caused by pore size increasing. As seen in Fig. 6(b), (c), (f) and (g), the interlayer spacing of recovered graphite is much larger and more obvious than that of spent graphite before acid leaching. The pore size distribution in Fig. 6 (i) further demonstrates that the average pore diameter of graphite increases from 11.6 nm to 13.5 nm. According to reported results, the expansion of the interlayer spacing of graphite always results in enhancement of high lithium storage capacities (Winter et al., 1998; Kim et al., 2014).

Coin cells were assembled to measure the lithiation/delithiation properties of regenerative graphite. The charge/discharge curves in Fig. 7 show the typical lithium de/intercalation plateau of graphite. Fig. 7(b) shows the step-by-step intercalation into graphite, which has been widely reported as a general feature of lithium intercalation into graphite, further proving the generation of graphite. Meanwhile, the first two discharge capacities at the current density of 37.2 mA·g^{-1} can reach 591 mAh·g^{-1} and 578 mAh·g^{-1}, respectively (Fig. 7(a)), much higher than the theoretical capacity of graphite (372 mAh·g^{-1}). To explain the higher specific capacity, several studies have been performed. Matsumura et al. reported that in addition to the lithium located between the graphene layers, plenty of lithium was stored on the edges and surfaces of graphite, and thus the graphite with small particle size has larger capacity of storing lithium (Matsumura et al., 1995). Yata et al. believed that higher interlayer spacings made LiC_2 formation in carbon more possible to occur (Yata et al., 1994). Dahn et al. suggested that lithium is "adsorbed" on both sides of single-layer sheets that are arranged like a "house of cards" or like "falling cards". The "falling cards" model is the advanced form of the "house of cards" model and also regards the storage of lithium in

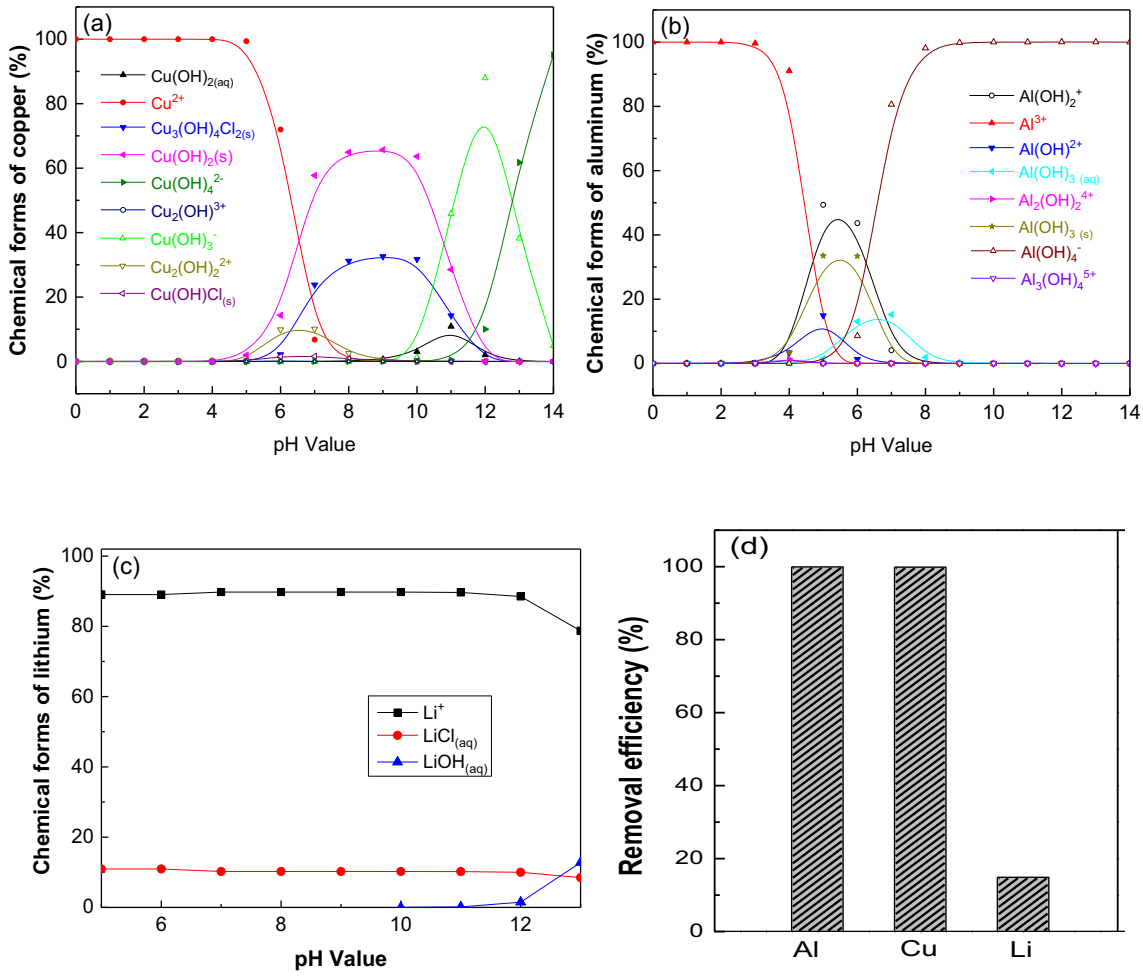

Fig. 4. Chemical forms of (a) copper (585 mg·L^{-1}), (b) aluminium (325 mg·L^{-1}) and (c) lithium (325 mg·L^{-1}) species as a function of pH value and (d) the removal efficiency of copper, aluminum and lithium after precipitation experiment.

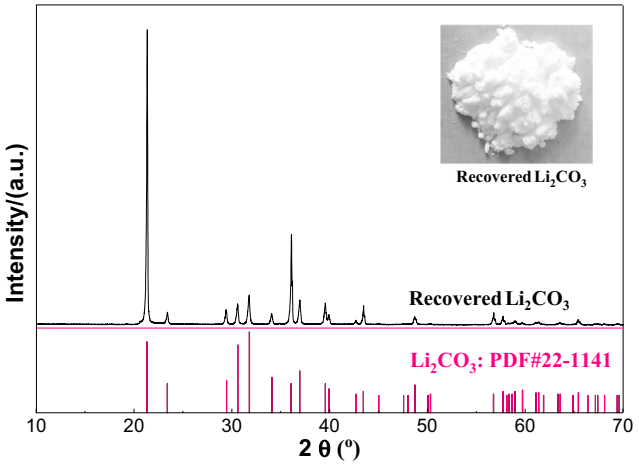

Fig. 5. XRD pattern of recovered lithium carbonate.

micropores (Winter et al., 1998; Xue and Dahn, 1995). All above explanations involve the particle size and pore size of graphite. Therefore, the specific capacity increase of regenerative graphite may be caused by the fact that the size of regenerated graphite becomes thinner and smaller but the interlayer spacing and pore size increase.

Fig. 8 displays the rate capability and cycle performance of regenerative graphite. As seen from Fig. 8(a), the overpotential increases with raising rate. This well agrees with reported results. The discharge capacities are 540–591 mAh·g^{-1}, 485–510 mAh·g^{-1}, 305–335 mAh·g^{-1} and 165–190 mAh·g^{-1} at corresponding current densities of 37.2 mA·g^{-1}, 74.4 mA·g^{-1}, 186 mA·g^{-1} and 372 mA·g^{-1}, respectively. Fig. 8(b) shows the cycle performance of regenerated graphite in the range of 0.01–2.0 V (vs Li$^+$/Li) at the current density of 372 mA·g^{-1}. After 100 cycles, the discharge capacity keeps at 166.6 mA·g^{-1} and the coulombic efficiency almost remains 100%. Compared with the initial discharge capacity of 172.6 mA·g^{-1}, the capacity retention ratio is 97.9% after 100 cycles. Fig. 9 shows the EIS measurement in the frequency ranging from 1 MHz to 0.01 Hz, both of EIS measured at the 1st and 100th cycle consist of a semicircle in the high frequency (representing the charge transfer resistance) and an approximate straight sloping line in the low frequency (representing lithium-ions diffusion process in electrodes). The diameter of the semicircle does not increase with the cycle number increasing, which means no increase in charge transfer resistance after 100 cycles with a current density of 372 mA·g^{-1}.

3.5. Waste management

Upon above analysis, the proposed process can recover lithium and regenerate graphite from spent LIBs, but it still depends on the

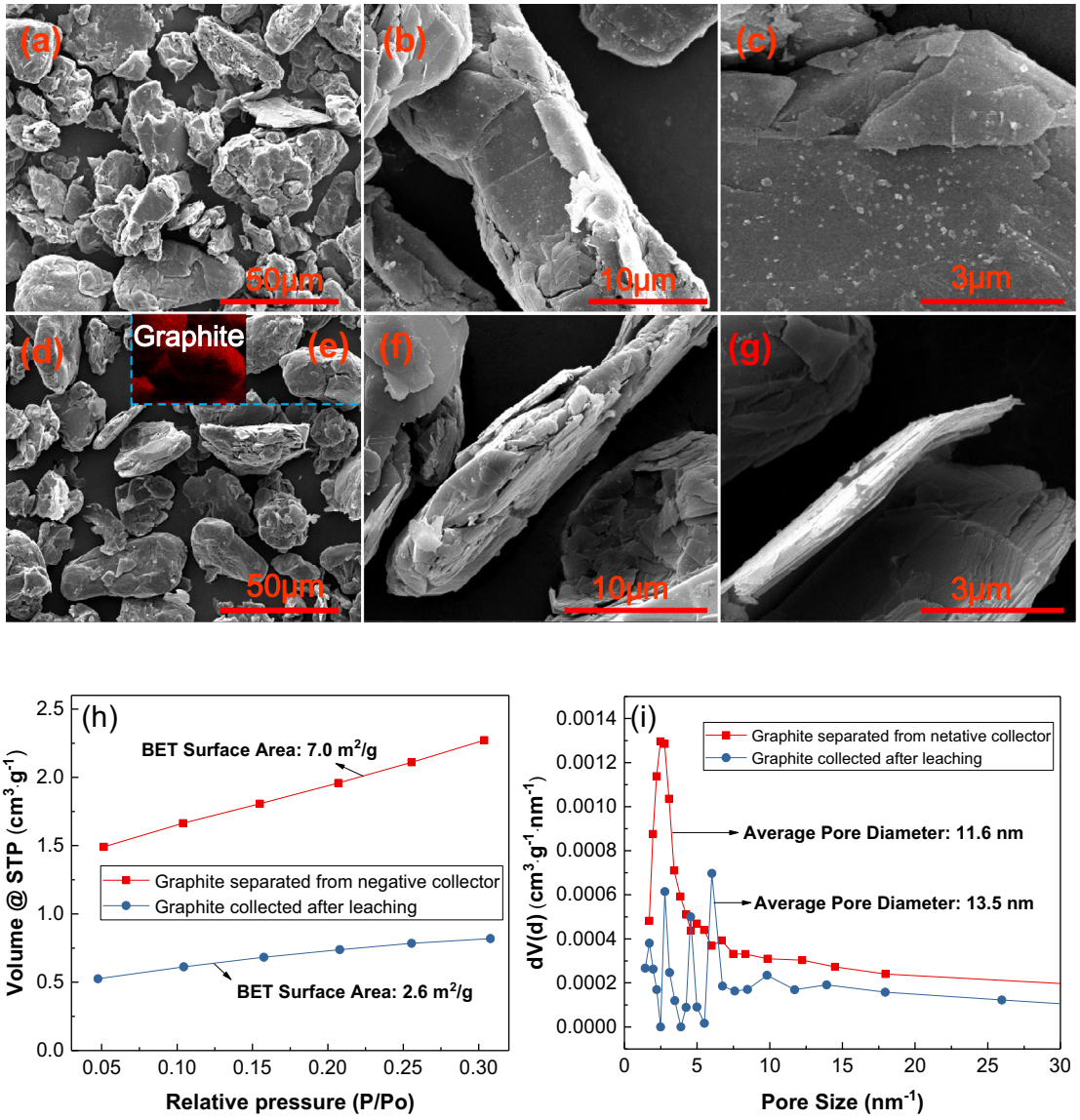

Fig. 6. (a)–(c) SEM images of spent graphite separated from anode current collector after thermal treatment at 500 °C for 1 h under air atmosphere; (d)–(g) SEM images and EDXS mapping of graphite recycled after acid leaching process under the condition of 1.5 M HCl, 60 min and S/L = 100 g·L^{-1}; (h) specific surface area and (i) pore size distribution of spent graphite separated from anode current collector (in images (a)–(c)) and graphite collected after acid leaching (in images (d), (f) and (g)).

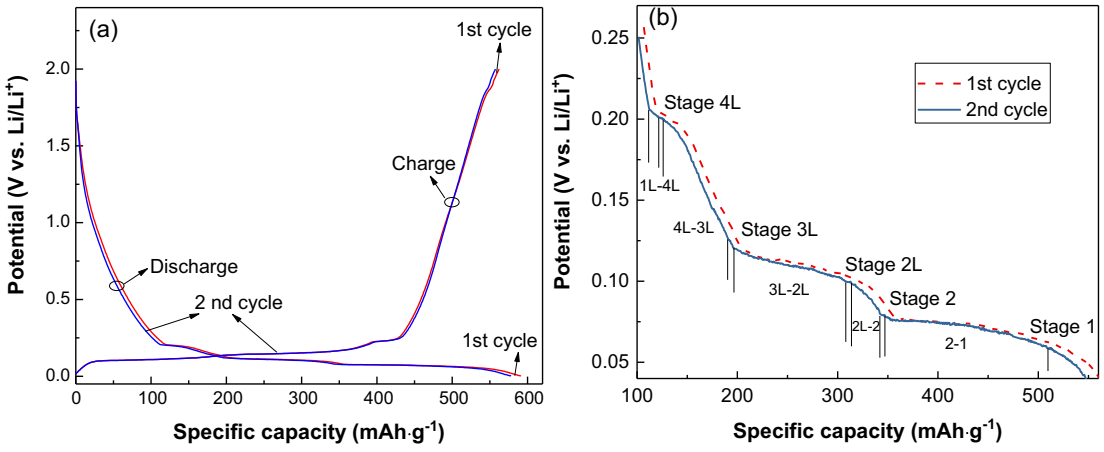

Fig. 7. (a) Initial and second charge and discharge profiles of regenerated graphite in the range of 0.01–2.0 V (vs Li^+/Li) with a current density of 37.2 mA·g^{-1} at 25 °C; (b) different lithium intercalation stages.

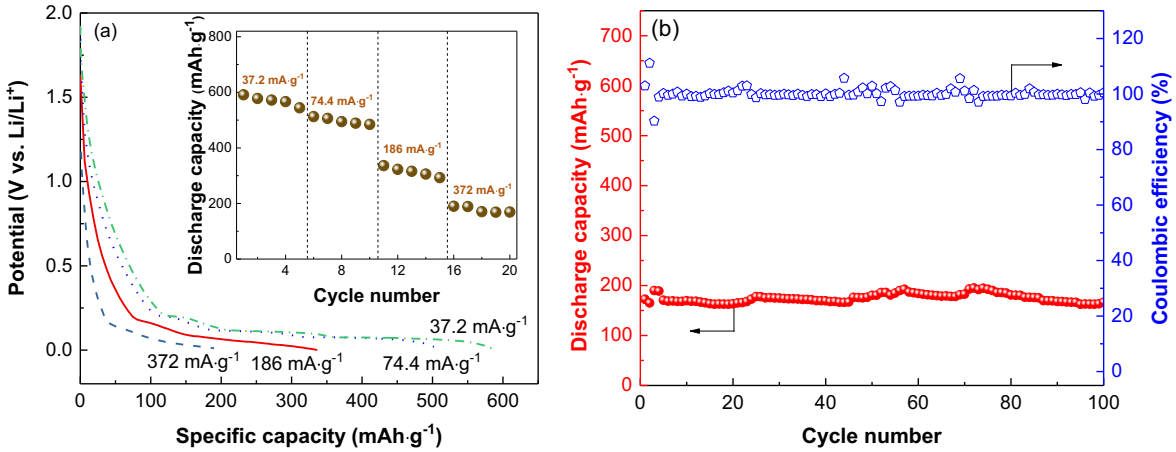

Fig. 8. (a) Rate capacities of regenerated graphite in the range of 0.01–2.0 V (vs Li^+/Li) with various current densities at 25 °C ; (b) cycle performance of regenerated graphite in the range of 0.01–2.0 V (vs Li^+/Li) with a current density of 372 mA·g^{-1} at 25 °C.

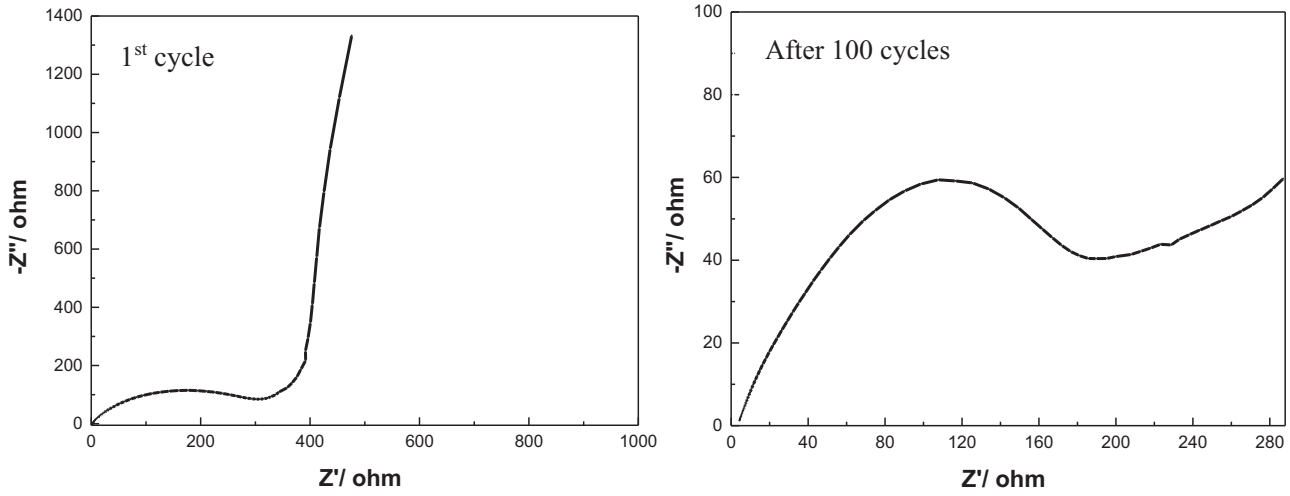

Fig. 9. Electrochemical impedance spectroscopy (EIS) of regenerated graphite in the frequency range from 1 MHz to 0.01 Hz at different cycles with a current density of 372 mA·g^{-1} at AC voltage of 5 mV.

effective management. On one hand, for a consideration of recycling spent graphite, the negative current collector and positive current collector must be separated effectively by a more precise separation method. Artificial separation can achieve this goal, but it is not enough to meet the requirements of industrial production. Therefore, machine separation is necessary. For the convenience of machine disassembly and accurate separation, the spent LIBs must be classified strictly according to materials, specifications, etc. (Pathak et al., 2017). On the other hand, the waste management during the whole recycling process should be considered. In the thermal treatment, it is reported that the electrolyte volatilizes and decomposes during the pyrolysis process (Rothermel et al., 2016). The harmful gases, such as hydrogen fluoride, organic compounds including ethylene carbonate, propylene carbonate or diethyl carbonate and their decomposed product, will be generated in the process of thermal treatment. However, these pollutions can be effectively eliminated by mature technology of alkali absorption followed by activated carbon adsorption (Senćanski et al., 2017; Xiao et al., 2017). In lithium recovery process, the precipitates of copper and aluminum can be further recovered by transferring to a professional processing facility. As HCl, NaOH and Na_2CO_3 employed, the alkali wastewater generated after lithium carbonate recovery. The alkali wastewater can simply be adjusted to pH = 6–7 and then reused for lithium leaching. After several cycles, the waste water can be distilled when the sodium content is near saturation.

Another issue for the recovery process is economy. For graphite can be seen as a waste product from the recycling of cathode materials, the transportation, discharge, disassembly and other costs should not be considered. Take the recovery of 1 t spent graphite for example, it consumes 1.644 t HCl, 0.602 t NaOH and 10, 000 KW·h power. The total cost is around 13, 364.2 CNY (Table S2). Currently, the price of 1 t graphite anode materials is about 15, 000 CNY. Moreover, there are copper metal and lithium carbonate products. Therefore, the recovery of graphite is economical.

4. Conclusion

To conclude, the whole process is simple and short, and can help achieve the comprehensive recovery of lithium and graphite, which enjoys great significance in sustainable development of LIBs.

(1) The spent graphite was firstly obtained by the two-stage calcination, and it suffered acid leaching to get the leach residue of graphite and the leach liquor. Approximately 100% lithium, copper and aluminum enter the leach liquor by acid

leaching under the conditions of 1.5 M HCl, 60 min and S/L = 100 g·L^{-1}, thus obtaining regenerative graphite with high purity. The regenerated graphite boasts impressive electrochemical properties. The initial specific capacities of regenerative graphite at the rates of 37.2 mA·g^{-1}, 74.4 mA·g^{-1} and 186 mA·g^{-1} were 591 mAh·g^{-1}, 510 mAh·g^{-1}, 335 mAh·g^{-1}, respectively, and its coulombic efficiency and capacity retention ratio almost remain 100% and 97.9%, respectively, after 100 cycles at a high rate of 372 mA·g^{-1}.

(2) Lithium in the leach liquor was recovered by carbonate precipitation method, and the purity of the recovered lithium carbonate was over 99%.

Acknowledgement

This work was supported by the Scientific Research Starting Foundation of Central South University (202045006). Key Laboratory of Hunan Province for Clean and Efficient Utilization of Strategic Calcium-containing Mineral Resources (2018TP1002).

Appendix A. Supplementary data

Supplementary data to this article can be found online at https://doi.org/10.1016/j.wasman.2019.01.008.

References

Alhusaiki, A.H.M., 2017. Thermal and electrical properties of graphene incorporated into polyvinylidene fluoride/polymethyl methacrylate nanocomposites. Polym. Compos. 38, E246–E253.
Altass, H., Carley, A.F., Davies, P.R., Davies, R.J., 2016. XPS and STM studies of the oxidation of hydrogen chloride at Cu(100) surfaces. Surf. Sci. 650, 177–186.
Badawy, S.M., 2016. Synthesis of high-quality graphene oxide from spent mobile phone batteries. Environ. Prog. Sustain. 35, 1485–1491.
Cao, Z., Zheng, X., Cao, H., Zhao, H., Sun, Z., Guo, Z., Wang, K., Zhou, B., 2018. Efficient reuse of anode scrap from lithium-ion batteries as cathode for pollutant degradation in electro-Fenton process: role of different recovery processes. Chem. Eng. J. 337, 256–264.
Chen, X.P., Cao, L., Kang, D.Z., Li, J.Z., Zhou, T., Ma, H.R., 2018. Recovery of valuable metals from mixed types of spent lithium ion batteries. Part II: selective extraction of lithium. Waste Manage. 80, 198–210.
Clark, M.M., Srivastava, R.M., David, R., 1993. Mixing and aluminum precipitation. Environ. Sci. Technol. 27, 2181–2189.
Duan, J., Gregory, J., 2003. Coagulation by hydrolysing metal salts. Adv. Colloid Interface Sci. 100–102, 475–502.
Gao, W.F., Zhang, X.H., Zheng, X.H., Lin, X., Cao, H.B., Zhang, Y., Sun, Z., 2017. Lithium carbonate recovery from cathode scrap of spent lithium-ion battery: a closed-loop process. Environ. Sci. Technol. 51, 1662–1669.
Gao, W.F., Liu, C.M., Cao, H.B., Zheng, X.H., Lin, X., Wang, H.Z., Zhang, Y., Sun, Z., 2018. Comprehensive evaluation on effective leaching of critical metals from spent lithium-ion batteries. Waste Manage. 75, 477–485.
Gomaa, H., Shenashen, M.A., Yamaguchi, H., Alamoudi, A.S., El-Safty, S.A., 2018. Extraction and recovery of Co^{2+} ions from spent lithium-ion batteries using hierarchical mesosponge gamma-Al_2O_3 monolith extractors. Green Chem. 20, 1841–1857.
Hou, H., Qiu, X., Wei, W., Zhang, Y., Ji, X., 2017. Carbon anode materials for advanced sodium-ion batteries. Adv. Energy Mater. 7, 1602898.
Kim, T.H., Jeon, E.K., Ko, Y., Jang, B.Y., Kim, B.S., Song, H.K., 2014. Enlarging the d-spacing of graphite and polarizing its surface charge for driving lithium ions fast. J. Mater. Chem. A 2, 7600–7605.
Lewis, E.E., Naylor, M.A., 1947. Pyrolysis of polytetrafluoroethylene. J. Am. Chem. Soc. 69, 1968–1970.
Li, L., Fan, E.S., Guan, Y.B.A., Zhang, X.X., Xue, Q., Wei, L., Wu, F., Chen, R.J., 2017. Sustainable recovery of cathode materials from spent lithium-ion batteries using lactic acid leaching system. ACS Sustain. Chem. Eng. 5, 5224–5233.
Li, J., Wang, G.X., Xu, Z.M., 2016. Generation and detection of metal ions and volatile organic compounds (VOCs) emissions from the pretreatment processes for recycling spent lithium-ion batteries. Waste Manage. 52, 221–227.
Lv, W.G., Wang, Z.H., Cao, H.B., Zheng, X.H., Jin, W., Zhang, Y., Sun, Z., 2018a. A sustainable process for metal recycling from spent lithium-ion batteries using ammonium chloride. Waste Manage. 79, 545–553.
Lv, W.G., Wang, Z.H., Cao, H.B., Sun, Y., Zhang, Y., Sun, Z., 2018b. A critical review and analysis on the recycling of spent lithium-ion batteries. ACS Sustain. Chem. Eng. 6, 1504–1521.
Matsumura, Y., Wang, S., Mondori, J., 1995. Interactions between disordered carbon and lithium in lithium ion rechargeable batteries. Carbon 33, 1457–1462.
Moradi, B., Botte, G., 2016. Recycling of graphite anodes for the next generation of lithium ion batteries. J. Appl. Electrochem. 46, 123–148.
Pankaj, K.C., Chung, K.S., Kim, M., Lee, J.C., Srivastava, R.R., 2017. Advance review on the exploitation of the prominent energy-storage element Lithium. Part II: from sea water and spent lithium ion batteries (LIBs). Miner. Eng. 110, 104–121.
Pathak, P., Srivastava, R.R., Ojasvic, 2017. Assessment of legislation and practices for the sustainable management of waste electrical and electronic equipment in India. Renew. Sustain. Energy Rev. 78, 220–232.
Rothermel, S., Evertz, M., Kasnatscheew, J., Qi, X., Gretzke, M., Winter, M., Nowak, S., 2016. Graphite recycling from spent lithium ion batteries. ChemSusChem 9, 3473–3484.
Sattar, R., Ilyas, S., Bhatti, H.N., Ghaffar, A., 2019. Resource recovery of critically-rare metals by hydrometallurgical recycling of spent lithium ion batteries. Sep. Purif. Technol. 209, 725–733.
Senćanski, J., Bajuk-Bogdanović, D., Majstorović, D., Tchernychova, E., Papan, J., Vujković, M., 2017. The synthesis of Li(Co-Mn-Ni)O2 cathode material from spent-Li ion batteries and the proof of its functionality in aqueous lithium and sodium electrolytic solutions. J. Power Sour. 342, 690–703.
Schweidler, S., Biasi, L., Schiele, A., Hartmann, P., Brezesinski, T., Janek, J., 2018. Volume changes of graphite anodes revisited: a combined operando X-ray diffraction and in situ pressure analysis study. J. Phys. Chem. C 122, 8829–8835.
Shaw, S., 2012. Increasing demand for high purity natural graphite in new applications. Natural & Synthetic Graphite: Global Industry Markets & Outlook, eighth ed.
Sun, W., Wang, L.D., Yang, Z.Q., Zhu, T.Z., Wu, T.T., Dong, C., Liu, G.C., 2018. Tuning the oxidation degree of graphite toward highly thermally conductive graphite/epoxy composites. Chem. Mater. 2018 (30), 7473–7483.
Tripathi, A.M., Su, W.N., Hwang, B.J., 2018. In situ analytical techniques for battery interface analysis. Chem. Soc. Rev. 47, 736–851.
U.S. Geological Survey, 2018. Mineral Commodity Summaries.
Wen, Y., He, K., Zhu, Y.J., Han, F.D., Xu, Y.H., Matsuda, I., Ishii, Y., Cumings, J., Wang, C. S., 2015. Expanded graphite as superior anode for sodium-ion batteries. Nat. Commun. 5, 4033.
Xiao, J.F., Li, J., Xu, Z.M., 2017. Novel approach for in situ recovery of lithium carbonate from spent lithium ion batteries using vacuum metallurgy. Environ. Sci. Technol. 51, 11960–11966.
Winter, M., Besenhard, J.O., Spahr, M.E., Novμk, P., 1998. Insertion electrode materials for rechargeable lithium batteries. Adv. Mater. 10, 725–763.
Xu, C., Yang, W., Liu, W., Sun, H., Jiao, C., Lin, A., 2018. Performance and mechanism of Cr(VI) removal by zero-valent iron loaded onto expanded graphite. J. Environ. Sci. 67, 14–22.
Xue, J.S., Dahn, J.R., 1995. Dramatic effect of oxidation on lithium insertion in carbons made from epoxy resins. J. Electrochem. Soc. 142, 3668–3677.
Yang, Y., Huang, G., Xu, S., He, Y., Liu, X., 2016a. Thermal treatment process for the recovery of valuable metals from spent lithium-ion batteries. Hydrometallurgy 165, 390–396.
Yang, Y., Song, S.L., Jiang, F., Zhou, J.H., Sun, W., 2018a. Short process for regenerating Mn-rich cathode material with high voltage from mixed-type spent cathode materials via a facile approach. J. Clean. Prod. 186, 123–130.
Yang, Y., Sun, W., Bu, Y.J., Zhang, C.Y., Song, S.L., Hu, Y.H., 2018b. Recovering valuable metals from spent lithium ion battery via a combination of reduction thermal treatment and facile acid leaching. ACS Sustain. Chem. Eng. 6, 10445–10453.
Yang, Y., Xu, S., He, Y., 2017. Lithium recycling and cathode material regeneration from acid leach liquor of spent lithium-ion battery via facile co-extraction and co-precipitation processes. Waste Manage. 64, 219–227.
Yang, Y., Huang, G., Xie, M., Xu, S., He, Y., 2016b. Synthesis and performance of spherical $LiNi_xCo_yMn_{1-x-y}O_2$ regenerated from nickel and cobalt scraps. Hydrometallurgy 165, 358–369.
Yata, S., Kinoshita, H., Komori, N., Ando, N., Kashiwamura, T., Harada, T., Tanaka, K., Yamabe, T., 1994. Structure and properties of deeply Li-doped polyacenic semiconductor materials beyond C6Li stage. Synth. Met. 62, 153–158.
Zhao, T., Yao, Y., Wang, M.L., Chen, R.J., Yu, Y.J., Wu, F., Zhang, C.Z., 2017. Preparation of MnO-modified graphite sorbents from spent Li-ion batteries for the treatment of water contaminated by lead, cadmium, and silver contaminated water treatment. ACS Appl. Mater. Inter. 9, 25369–25376.
Zou, H.Y., Gratz, E., Apelian, D., Wang, Y., 2013. A novel method to recycle mixed cathode materials for lithium ion batteries. Green Chem. 15, 1183–1191.